



Universiteit Utrecht

UTRECHT UNIVERSITY

INSTITUTE FOR THEORETICAL PHYSICS

BACHELOR'S THESIS

Modelling Charge-selective Membranes Using Poisson-Nernst-Planck Equations

Author:
Sander KOOI

Supervisors:
Prof. Dr. René van ROIJ
Dr. Andreas HÄRTEL
Mathijs JANSSEN, M.Sc.
Dr. Sela SAMIN

June 2014

Abstract

Charge-selective membranes play an important role in reverse electro dialysis (RED), which is a process to extract energy from the mixing of fresh and salt water. This thesis begins by deriving the classical limiting current for charge-selective membranes. We then look at modelling a charge-selective membrane using the Poisson-Nernst-Planck system and solve this system numerically. We find results in agreement with the literature, including the emergence of a so called extended space charge. Lastly other literature on the dynamics of currents through a membrane and additional physical mechanism causing over-limiting current are briefly discussed.

Acknowledgements

I would like to thank René van Roij, Andreas Härtel, Mathijs Janssen, Sela Samin, Peter Cats and Jurriaan Wouters for their help in writing this thesis, for their patience in explaining me physical concepts, for the help in hunting down countless bugs and for the fruitful discussions every Tuesday morning.

Contents

1	Introduction	2
2	Microscopic origin of charge-selective membranes	4
3	Theory	6
3.1	Single membrane wall	6
3.2	Poisson Nernst-Planck system	10
4	Numerical solutions	13
4.1	Method	13
4.1.1	Finite difference method	14
4.1.2	Unequal spacing	15
4.1.3	Iterative steps	16
4.2	Results	17
4.2.1	Extended space charge	19
5	Conclusion and discussion	22

1 Introduction

Energy is slowly but surely becoming a more expensive good in our society due to the depletion of natural resources and the bad reputation of nuclear power. For this reason, and because traditional ways of generating energy are usually very polluting, finding renewable energy sources is an important and extremely active field of research. One way of generating clean energy is from a salinity-gradient or 'blue engine' [1]. A blue engine can extract energy from a salinity-gradient, which naturally occurs when a river (fresh water) ends in the sea (salt water). Energy is released because water containing a high salt-concentration mixes with water with a low salt-concentration, this energy is equal to water falling from 280m [2]. A theoretical maximum efficiency cycle has recently been found for this engine [3], and more generally mixing energy can be extracted from any process in which a high-concentration solution mixes with a low-concentration solution. Another concentration-gradient engine which was recently proposed is one that extracts energy from the mixing of CO₂-enriched water with fresh water, using a similar method as some of the salinity-gradient engines [4]. A theoretical outline has also been published [5].

There are three ways in which these types of concentration-gradient engines are currently being implemented [3]. The first is pressure-retarded osmosis (PRO). In this method a semi-permeable membrane, allowing water but no ions to go through, is placed between a high-salt and a low-salt solution. Osmotic pressure will cause water to flow from the low-salt to the high-salt solution and this can power for example a hydraulic pump or turbine [6]. A second method, proposed by Brogioli [7], does not use membranes at all. Two porous carbon electrodes are placed on both sides of a flush channel, salt water is brought in and a voltage is applied across the system, charging the electrodes. The salt water is then replaced with fresh water, leading the salt-ions to diffuse away from the capacitors. This increases the voltage and results in net energy production when the capacitors are discharged.

A third method, on which the focus will lie in this thesis, is reverse electro dialysis (RED). This method uses both membranes and electrodes. A cation-exchange and an anion-exchange membrane, with electrodes behind them, are placed on opposite sides of, for example, a high-salt solution. The ions and co-ions will diffuse through different membranes, creating a voltage across the system and charging the electrodes. When the high-salt solution is flushed and replaced with pure water, the electrodes will discharge. In both these steps a (non-constant) current will flow between the two electrodes. In practice 'stacks' of RED cells are used to increase efficiency as shown in Figure 1 [8]. In normal conditions a power density of 3.5 W /

m^2 can theoretically be obtained using RED stacks [9]. In practice power densities of $0.9 \text{ W} / \text{m}^2$ have been obtained [8], and a RED power-plant is currently being build in the Netherlands. In this thesis we will examine how we can model a charge-selective membrane using the Poisson-Nernst-Planck system of equations, and determine what the characteristics of this model are. In section 2 the microscopic origin of charge selectivity will briefly be discussed. In section 3 we will discuss the equations we can use to model a charge-selective membrane and see what we can analytically learn from these equations. In section 4 numerical results will be shown and analysed and in section 5 conclusions will be given and other models and experimental findings will be discussed.

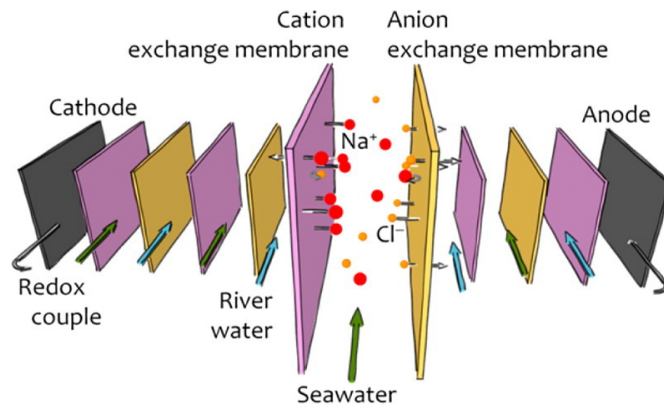


Figure 1: Schematic drawing of a RED stack. Source: [9]

2 Microscopic origin of charge-selective membranes

Synthesized charge selective membranes are usually made of polymers. Surface groups of these polymers will react with water and become charged, thus creating fixed charges. We can then describe a two-dimensional membrane as having a thickness L , n pores with a typical pore width d and a porosity $p = V_{\text{free}}/V_{\text{total}}$, where $V_{\text{free}} = ndL$ is the volume in the membrane available to the solution and V_{total} is the total volume of the membrane. The membrane will carry a charge density of σ on the pore surface. The average charge density of the membrane is then $Q = \frac{2nLe\sigma}{V_{\text{tot}}} = \frac{2pe\sigma}{d}$. Let us now think of this membrane as submerged in an ionic solution. There are then two reservoirs with an ionic concentration of C_{res} on both sides of the membrane. Two regimes of selectivity can be distinguished. For $C_{\text{res}} \gg \bar{Q}$, the membrane charge will be easily screened and the solution in the majority of the pore will be electro-neutral. This corresponds to wide pores compared to the length-scale over which charge imbalances occur, this length-scale is called the Debye length. The membrane will be poorly selective in this case, as no electric field is deterring negatively charged particles from flowing through the majority of the pore. When $C_{\text{res}} \ll \bar{Q}$ the double layers of the pore sides will overlap strongly, and the membrane will be highly selective. The Debye length is in this case large compared to the width of the pore, and a large electric field in the pores will deter negatively charged particles from flowing through. Both regimes of selectivity and the set-up is shown in Figure 2. In the rest of this thesis we will only look at a the one dimensional Poisson-Nernst-Planck system. We will treat a membrane as a fixed charge density, and thus we will not take into effect any screening of the pores in the z -direction. This means that we will consider the case of strongly overlapping double layers. This seems reasonable, as we are interested in the case where the membrane is charge-selective.

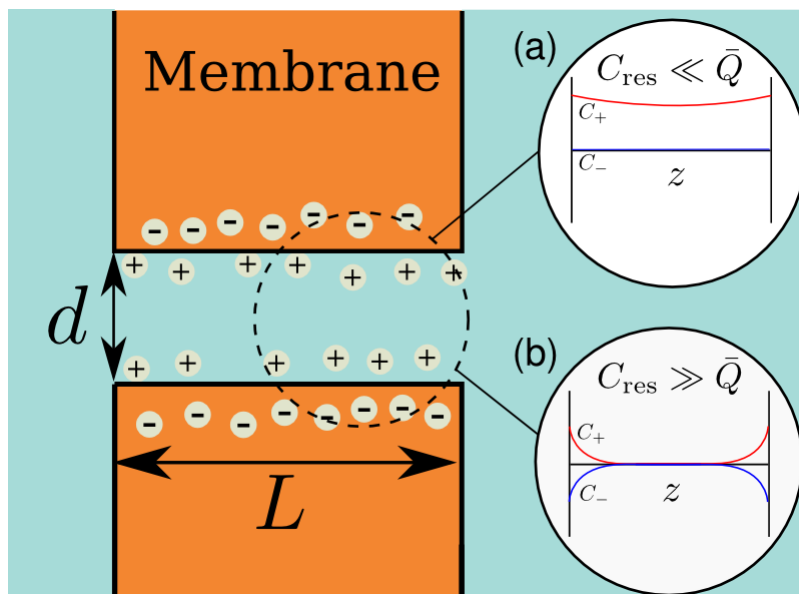


Figure 2: Schematic picture of a pore (of width d) in a negatively charged membrane. This pore contains a net positive charge and is in contact with a reservoir on both sides. (a) shows the concentration profiles for a highly selective membrane, where there are strongly overlapping double layers and almost no negative charges are present in the pore. (b) shows a poorly selective membrane where the membrane charge is screened easily and the majority of the pore is electro-neutral.

3 Theory

3.1 Single membrane wall

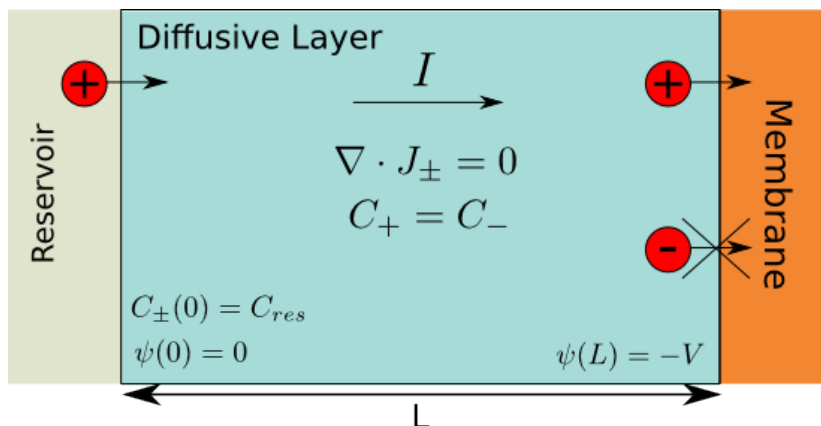


Figure 3: Diagram of the single wall model. The diffusive layer is connected to a reservoir on the left and a membrane on the right. Negatively charged particles cannot go through the membrane.

This section largely follows [10]. Let us consider a simple system consisting of a solution with positively and negatively charged particles, and a membrane placed at a constant potential $-V$ as shown in Figure 3. This membrane allows only positively charged particles to go through. We will consider steady-state solutions (that is, a constant current). In this system there will be a constant flow of positive particles, while the negatively charged particles will not flow. The flux in this system is

$$J_{\pm}(x) = -D_{\pm} \left(\frac{dC_{\pm}(x)}{dx} \mp C_{\pm}(x) \frac{d\phi(x)}{dx} \right), \quad (1)$$

where $\phi = \frac{e}{k_B T} \psi$ is the dimensionless potential with ψ the original potential in volts, C_{\pm} is the concentration, D_{\pm} is the diffusion constant and J_{\pm} is the flux of the positive and negative particles. The flux is a combination of diffusion (dependent on the gradient of the concentration) and electro migration (dependent on the gradient of the potential). An assumption we can make is that our electrolyte is quasi-neutral, with $C_+ = C_-$. We expect this to be the case far away from the membrane wall. This is because the ions in our system will screen the charged membrane wall and thus there will form a double-layer with the length in the order of the Debye length, which is typically a few nanometres. The electro-neutrality assumption will thus be a good approximation away from the membrane interface.

We place our membrane at a distance $x = L$ and a reservoir with concentration C_{res} at $x = 0$. Between the reservoir and the membrane there will be a diffusive layer, the region in which particles will diffuse towards the membrane. At the interface of the reservoir and the diffusive layer there will be no diffusion and across the entire system a voltage will be applied. This geometry imposes the boundary conditions

$$\phi(0) = 0, \quad C_{\pm}(0) = C_{res}, \quad \phi(L) = -V, \quad (2)$$

where C_{res} is the concentration in the reservoir, L is the length of the diffusive layer and voltage applied across the system is $-V$ where V is positive. Now since the negative particles do not flow, they will be in chemical equilibrium with the reservoir. This means that their chemical potentials are equal. The chemical potential is given by

$$\frac{\mu_{\pm}}{k_B T} = \ln C_{\pm}(x) \pm \phi(x). \quad (3)$$

Since $\phi = 0$ in the reservoir and $C_{res} = cst.$, it follows that μ_{res} is also constant and we get

$$\frac{\mu_{-}}{k_B T} = \ln(C_{-}(x)) - \phi(x) = \ln(C_{res}(x)), \quad (4)$$

$$\phi(x) = \ln\left(\frac{C_{-}(x)}{C_{res}}\right) = \ln\left(\frac{C_{+}(x)}{C_{res}}\right), \quad (5)$$

Where we used the electro-neutrality assumption. Now we can calculate the current flowing in this system:

$$I = eJ_{+}A = -eAD_{+}\left(\frac{dC_{+}}{dx} + C_{+}\frac{d\phi}{dx}\right), \quad (6)$$

where A is the area of the membrane. Setting $c = \frac{C_{\pm}}{C_{res}}$ and $\bar{x} = \frac{x}{L}$ we can rewrite (6) using (5) to get

$$I = -\frac{eAC_{res}}{L}D_{+}\left(\frac{dc}{d\bar{x}} + c\frac{d\phi}{d\bar{x}}\right) = -2\frac{eAC_{res}}{L}D_{+}\frac{dc}{d\bar{x}}. \quad (7)$$

Our solution will have a constant current and therefore $dc/d\bar{x}$ is constant. Since $c(0) = 1$ and $c(L) \geq 0$, the maximum value of $dc/d\bar{x} = 1$. The limiting current is then defined as

$$I_{lim} = 2\frac{eAC_{res}}{L}D_{+}. \quad (8)$$

The equations for the (dimensionless) concentration and potential can then also be rewritten in terms of the dimensionless current

$$\bar{I} = \frac{I}{I_{\text{lim}}} = -\frac{dc}{d\bar{x}}. \quad (9)$$

Integrating this expression using our boundary conditions (2) we get

$$c(x) = 1 - \bar{I}\bar{x} \quad (10)$$

and substituting this into (5) gives

$$\phi(x) = \ln(1 - \bar{I}\bar{x}). \quad (11)$$

This is plotted for various currents in Figure 4. As the current approaches the limiting current, we observe that $c(L) \rightarrow 1$ and $\phi(L) \rightarrow \infty$. Thus at the interface of the membrane and the electrolyte the concentration of particles will drop to zero, this means that every particle will immediately be absorbed by the membrane. One final remark we can make about this system is that it has the same I-V characteristics as a diode. Rewriting equation (11) gives

$$\phi(L) = \ln(1 - \bar{I}) = -\frac{eV}{k_{\text{B}}T} \quad (12)$$

$$\Rightarrow \bar{I} = 1 - e^{-\frac{eV}{k_{\text{B}}T}}, \quad (13)$$

which is plotted in Figure 5.

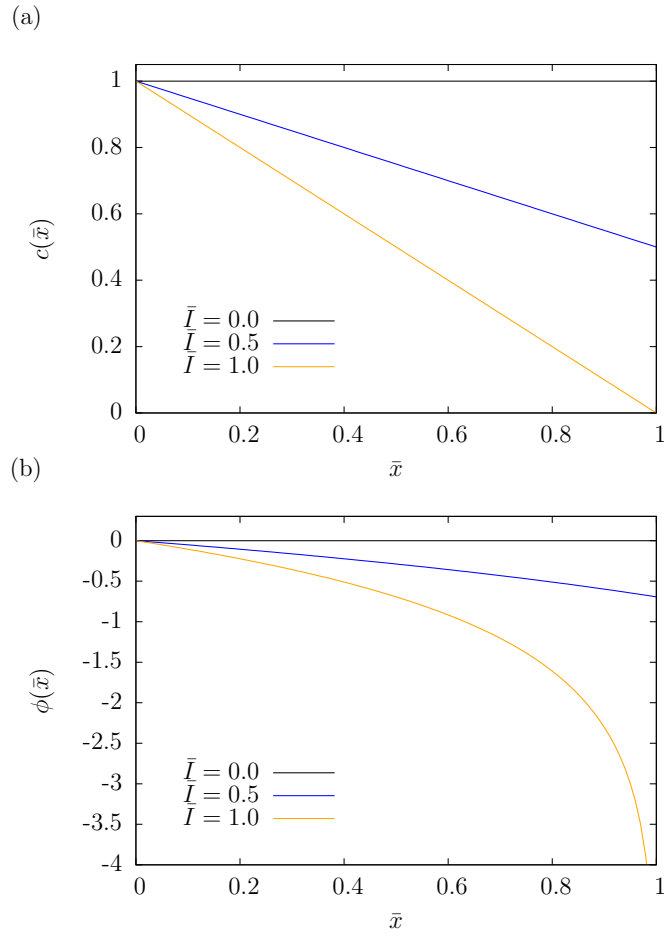


Figure 4: The concentrations (a) and potential (b) plotted for various values of the dimensionless current.

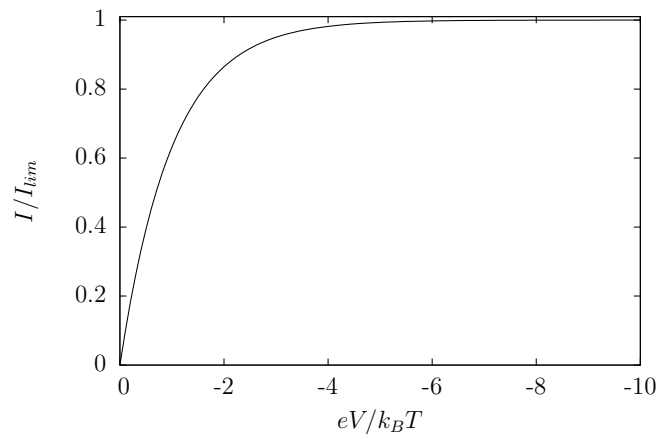


Figure 5: The I-V curve, plot of equation (13). For low voltages we see a linear regime.

3.2 Poisson Nernst-Planck system

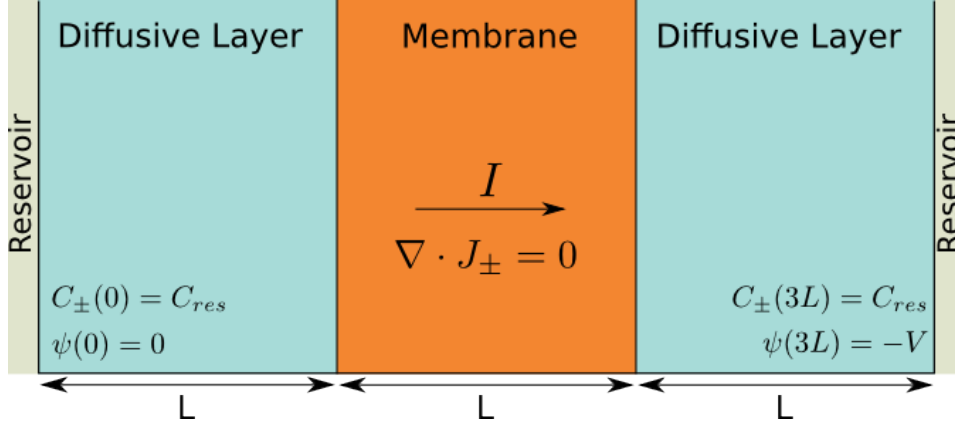


Figure 6: Our second model. A membrane with diffusive layers on both sides. The membrane is modelled as a fixed charge density in the center, both positive and negative particles are allowed to pass through.

We now turn to the dynamics of a current flowing through a membrane with reservoirs on both sides. The system we will consider consists of a membrane of thickness L between two diffusive layers, also of thickness L . The membrane is modelled as a region which has a fixed charge density of Q . This is a more realistic approach than the one we used in the last section, where the membrane was assumed to be impenetrable to anions, as membranes are usually realized as charged polymers. Anions are now allowed to go through the membrane, but will be deterred by the negative charge already present. Across this system again a voltage is applied of $-V$ where V is positive. This system is thus a cation-selective membrane. If we would apply a positive voltage and if our membrane was positively charged, we would have an anion-selective membrane. The equations describing this system are the 1D Nernst-Planck equation

$$\frac{dc_{\pm}}{dt} = -\nabla \cdot J_{\pm}, \quad (14)$$

where

$$J_{\pm}(x) = -D_{\pm} \left(\frac{dC_{\pm}}{dx} \mp C_{\pm}(x) \frac{e}{k_B T} \frac{d\psi}{dx} \right), \quad (15)$$

and the 1D Poisson equation

$$\frac{d^2\psi}{dx^2} = -\frac{4\pi e}{\epsilon} (C_+(x) - C_-(x) + Q(x)). \quad (16)$$

At the edges of the diffusive layers, e.g. on $x = 0$ and $x = 3L$, the concentrations of the cations and anions will be equal to that of the reservoir and the potential will be zero. This is by our definition of the diffusive layer as the region where there is no diffusion of particles, so (15) is equal to zero. This leads to six boundary conditions

$$C_{\pm}(0) = C_{\pm}(3L) = C_{res} \quad (17)$$

$$\psi(0) = 0; \psi(3L) = -V. \quad (18)$$

We will restrict ourselves to the steady-state solution in which the flux will be a spatial constant, which means in our geometry

$$\frac{dc_{\pm}}{dt} = -\frac{dJ_{\pm}}{dx} = 0. \quad (19)$$

The equations (14), (15) and (19), together with the boundary conditions (17) and (18), form a closed set of equations which we solve numerically in the next section. We can see that this set of equations also leads to the same limiting-current if we assume for a moment electro-neutrality. This means that (following [11])

$$C_+(x) = C_-(x), \quad (20)$$

and thus

$$J_+ + J_- = -2D\left(\frac{dC_+}{dx} + \frac{dC_-}{dx}\right) + (C_+ - C_-)\phi = -2D\frac{dC}{dx}, \quad (21)$$

from which we can write the concentrations in the left diffusive layer as

$$C_+(x) = C_-(x) = C_{res} - \frac{J_+ + J_-}{2D}x, \quad 0 \leq x < L, \quad (22)$$

because we know that both J_+ and J_- are constant and $C_{\pm}(0) = C_{res}$ in our steady-state model. Thus we find the concentrations decreasing linearly. We can now again find a limiting current by setting

$$C_{\pm}(L) = C_{res} - \frac{J_+ + J_-}{2D}L = 0 \quad (23)$$

and combining this with

$$I = e(J_+ - J_-)A \quad (24)$$

where A is the area. We can now combine (23) and (24) to obtain (following [11])

$$I_{lim} = 2DeA \frac{J_+ - J_-}{J_+ + J_-} \frac{C_{res}}{L} = 2DeA \frac{\alpha - 1}{\alpha + 1} \frac{C_{res}}{L}, \quad (25)$$

where we introduce $\alpha = \frac{J_+}{J_-}$, which is closely related to the selectivity of the membrane. If we take $\alpha \rightarrow \infty$ we get a membrane that does not allow any anions through and we see indeed that in this case (25) takes the form of (8).

When numerically solving the full PNP system (equations (16), (15), (17) and (18)) we are not able to set the membrane to be completely selective, because this will only be achieved in the limit $Q = \infty$ but only to finite values. We however observe larger currents when α is lower, thus contradicting (25). We will investigate this behaviour in the next section.

4 Numerical solutions

In this section the methodology and results of numerical solutions to equations (15), (16), (17) and (18) will be explained and presented. First we will make the equations dimensionless and cast them in a convenient form for our solving method. After this the solving method will be explained and the results shown.

4.1 Method

Let us begin by combining

$$\frac{dJ_{\pm}}{dx} = 0, \quad (26)$$

and

$$J_{\pm}(x) = -D_{\pm} \left(\frac{dC_{\pm}}{dx} \mp C_{\pm}(x) \frac{e}{k_{\text{B}}T} \frac{d\phi}{dx} \right), \quad (27)$$

to get the following equations

$$\frac{d^2C_{\pm}}{dx^2} \mp \frac{dC_{\pm}}{dx} \frac{e}{k_{\text{B}}T} \frac{d\phi}{dx} \mp C_{\pm}(x) \frac{e}{k_{\text{B}}T} \frac{d^2\phi}{dx^2} = 0. \quad (28)$$

We can introduce the following dimensionless quantities to further simplify this expression

$$\phi(x) = \frac{e}{k_{\text{B}}T} \psi(x); \quad c_{\pm}(x) = \frac{C_{\pm}(x)}{C_{\text{res}}}; \quad q(x) = \frac{Q(x)}{C_{\text{res}}}. \quad (29)$$

Rewriting equation (28) using these quantities we obtain

$$\frac{d^2c_{\pm}}{dx^2} = \pm \frac{dc_{\pm}}{dx} \frac{d\phi}{dx} \pm c_{\pm}(x) \frac{d^2\phi}{dx^2}. \quad (30)$$

We also have to express our other equation, the Poisson equation (16), in terms of our new variables. This gives

$$\frac{d^2\phi}{dx^2} = -\frac{4\pi\lambda_{\text{B}}}{C_{\text{res}}} (c_{+}(x) - c_{-}(x) + q(x)), \quad (31)$$

where $\lambda_{\text{B}} = \frac{\epsilon^2}{\epsilon k_{\text{B}}T}$ is the Bjerrum length. The Bjerrum length is the length scale at which electrostatic interactions occur in the system. We will use $\lambda_{\text{B}} = 0.72\text{nm}$ which is approximately the value of the Bjerrum length at room temperature in water. Finally, our boundary conditions will take the following form:

$$c_{\pm}(0) = c_{\pm}(3L) = 1, \quad (32)$$

$$\phi(0) = 0; \phi(3L) = -\frac{eV}{k_{\text{B}}T}. \quad (33)$$

Our system is now reduced to two second-order, non-linear differential equations, equations (30) and (31). In order to solve these we will use a finite-difference method in combination with the Thomas algorithm [12], as explained below.

4.1.1 Finite difference method

We will solve our system only on certain intervals, which we represent as a grid. We therefore want to calculate the derivative at a grid-point in terms of its neighbours. This method is called a finite-difference method and it can be derived by examining the Taylor expansion of a function [13]

$$f(x + \Delta x) = f(x) + f'(x)\Delta x + \frac{1}{2}f''(x)\Delta x^2 + \mathcal{O}(\Delta x^3) \quad (34)$$

$$f(x - \Delta x) = f(x) - f'(x)\Delta x + \frac{1}{2}f''(x)\Delta x^2 + \mathcal{O}(\Delta x^3) \quad (35)$$

Subtracting (35) from (34) gives (to first-order)

$$f'(x) = \frac{f(x + \Delta x) - f(x - \Delta x)}{2\Delta x} + \mathcal{O}(\Delta x^2), \quad (36)$$

and adding (34) and (35) gives (to second-order)

$$f''(x) = \frac{f(x + \Delta x) + f(x - \Delta x) - 2f(x)}{\Delta x^2} + \mathcal{O}(\Delta x^3). \quad (37)$$

Note that taking the derivative of (36) does not give us (37), doing this would give a different approximation. When we now have a grid of uniformly spaced points, we can take derivatives at these points using (36) and (37). Equations (30) and (31) can now be reduced to a set of linear equations, for example for the potential (31) we get

$$\phi(x + \Delta x) + \phi(x - \Delta x) - 2\phi(x) = -\frac{4\pi\lambda_{\text{B}}\Delta x^2}{C_{\text{res}}}(c_{+}(x) - c_{-}(x) + q(x)) \quad (38)$$

where Δx is taken to be the uniform distance between two grid-points. We get N (where N is the number of grid-points) coupled linear equations, which in matrix form look like

$$\begin{pmatrix} -2 & 1 & 0 & 0 \\ 1 & -2 & \ddots & 0 \\ 0 & \ddots & \ddots & 1 \\ 0 & 0 & 1 & -2 \end{pmatrix} \begin{pmatrix} \phi(1) \\ \phi(2) \\ \vdots \\ \phi(N) \end{pmatrix} = \begin{pmatrix} r(1) - \phi(0) \\ r(2) \\ \vdots \\ r(N) - \phi(N+1) \end{pmatrix}, \quad (39)$$

where $r(n)$ is the right-hand-side of equation (38). Notice that the first and last coordinate of the right-hand-side have an extra term corresponding to the boundary conditions. In our case the first coordinate will remain $r(1)$ while the last coordinate will be $r(N) + V$. We could in principle solve this equation by Gauss-Jordan elimination, but because our matrix is tridiagonal we can use the Thomas algorithm [12]. We can solve (30) in the same way, we then calculate the right-hand-side using the old values of C_+ and C_- and subtract 1 from the first and last term of the right-hand-side in (39) to account for the boundary conditions.

4.1.2 Unequal spacing

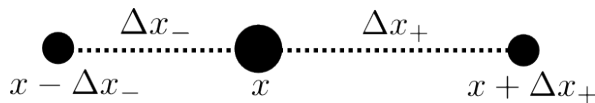


Figure 7: Schematic representation of an unequally spaced grid. We want to compute the derivative at x .

So far we have considered the spacing between our grid-points to be equal, and this made our result come out rather nicely because cancellations in the calculation. To increase convergence we would, however, like to implement an unequally spaced grid. In this case we will have to re-derive equations (36) and (37). We start by again Taylor expanding a function $f(x)$ at the neighbouring points, which are now at a distance Δx_+ and Δx_- as drawn in figure 7. This gives us [13]

$$f(x + \Delta x_+) = f(x) + f'(x)\alpha\Delta x_- + f''(x)\frac{(\alpha\Delta x_-)^2}{2} + \mathcal{O}(\Delta x^3), \quad (40)$$

and

$$f(x - \Delta x_-) = f(x) - f'(x)\Delta x_- + f''(x)\frac{(-\Delta x_-)^2}{2} + \mathcal{O}(\Delta x^3), \quad (41)$$

where we have introduced $\alpha = \frac{\Delta x_+}{\Delta x_-}$. To get an approximation for the first and second derivatives we need to take a linear combination of (40) and (41) in

such a way that we are left with the first and second derivatives respectively at the point x . Let us first calculate the first derivative. Taking a linear combination gives

$$af(x+\Delta x_+)+bf(x-\Delta x_-) = (a+b)f(x)+(a\alpha-b)f'(x)\Delta x_- + \frac{a\alpha^2+b}{2}f''(x)\Delta x_-^2. \quad (42)$$

To get a first order approximation we require the coefficient of f' to be 1 and the coefficient of f'' to be zero. This means that we get as conditions on a and b

$$a\alpha - b = 1; \quad a\alpha^2 + b = 0, \quad (43)$$

which is easily solved for a and b and substituted back into (42). After rearranging the result we get

$$f'(x) = \frac{f(x+1)\Delta x_-^2 - f(x-1)\Delta x_+^2 + f(x)(\Delta x_+^2 + \Delta x_-^2)}{\Delta x_+\Delta x_-(\Delta x_+ + \Delta x_-)}. \quad (44)$$

The same procedure can be followed to obtain the second derivative for an unequally spaced grid. In this case the Taylor expansion will need to be evaluated up to the third order. The result of this calculation is

$$f''(x) = \frac{f(x+1)\Delta x_- + f(x-1)\Delta x_+ - f(x)(\Delta x_+ + \Delta x_-)}{\Delta x_+\Delta x_-(\Delta x_+ + \Delta x_-)} \quad (45)$$

It is an easy check that when $\Delta x_+ = \Delta x_-$ we recover equation (37). We again have a set of linear equations, similar to (39). However, our matrix will have other values on the tri-diagonal and the right-hand side will also be multiplied by a different factor, both depending on Δx_+ and Δx_- . We have implemented a grid where we have a denser grid in an area δ around the membrane-diffusive layer interfaces. This means that we have four points at which we need to implement the unequal spacing, and thus adjust the matrix at these positions. We have chosen this grid because at the membrane-diffusive layer interfaces we will have the largest derivatives and problems of convergence will occur here fastest.

4.1.3 Iterative steps

We obtain our results in the following way: first, we provide an initial guess for C_+ and C_- . From this, we then solve (31) using the Thomas algorithm to obtain the potential. We then insert the potential into (30) and calculate the rest of the right-hand-side using the initial guess of C_+ and C_- . We can

then calculate the potential again from our new values of the concentration. To increase convergence we take a linear combination of the old and new values for some $\gamma \in [0, 1]$ in the following way:

$$C_{n+1} = (1 - \gamma)C_n + \gamma C_{calculated} \quad (46)$$

for both C_+ and C_- , where $C_{calculated}$ is the value of the concentration calculated and C_n is the old value of the concentration. This way we can ensure that the change in concentration is not too big from one iteration to the next and this decreases the chance of the results blowing up. The value of α was tweaked experimentally and changes for different values of L , V and q . For most results a length of $L = 333.0\text{nm}$ was used.

4.2 Results

Our system has two membrane-diffusive layer interfaces. Here, electric double layers will form. Far away from these double layers, for low voltages, the solution will be electro neutral. This means that from (31) the potential will be linear in these regions, and the concentration will also decrease linearly from (30). We can see this behaviour for small voltages and $q = Q/C_{res} = 5$ in Figure 8, where we plot the potential and concentrations for low voltages. We can also already see this behaviour breaking down and we will now take a closer look at the parameters we can tweak in this system, and their effects.

The first parameter we will look at is Q/C_{res} or q , the ratio of the membrane charge density to the reservoir concentration. This sets the selectivity of our membrane. If $Q < 0$ and $-Q \ll C_{res}$ then this means that negatively charged can flow through the membrane relatively easily. When $-Q \gg C_{res}$ the membrane will be highly selective. We expect our analytical limiting current (8) to be obtained for $-Q \gg C_{res}$ and high voltages. The obtained I-V diagram for different values of q is shown in Figure 9 at a membrane thickness of $L = 333.0\text{nm}$. We can see that indeed that the I-V curve for large negative q tends to get closer to the analytical limiting current, the limiting current is however exceeded very easily. This is because we do not have a perfectly selective membrane and we will thus also have a current of negative particles flowing in the opposite direction. The ratio of these two currents is plotted in Figure 10 for different values of q . We can also check our analytical expression for the current for non perfect selective membranes (25) against this diagram. For this we first need to know $\alpha = \frac{J_+}{J_-}$. We can however immediately see that the expression $\frac{\alpha-1}{\alpha+1}$ never becomes larger than one, and thus this analytical result predicts currents smaller than the limiting current which is clearly in disagreement with our findings in Figure 9.

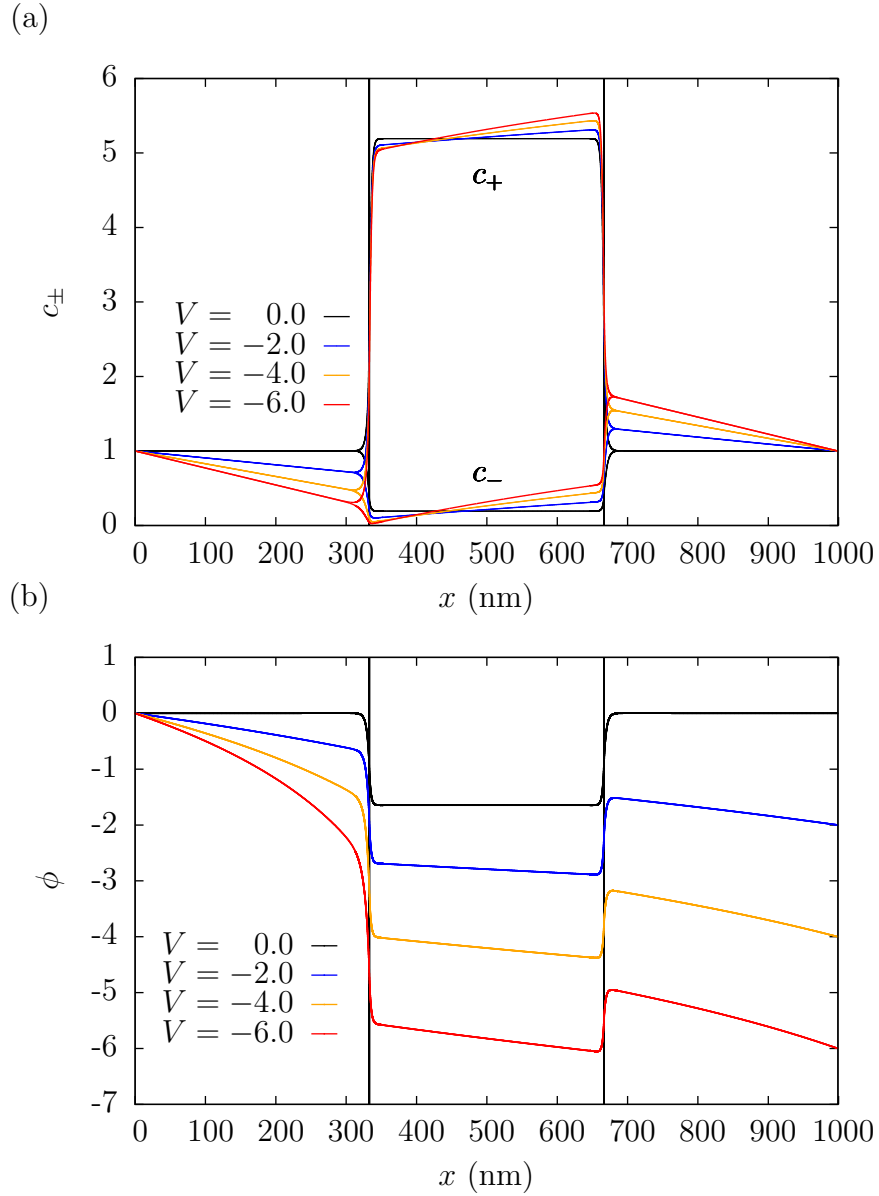


Figure 8: (a) The relative concentrations and (b) the dimensionless potential plotted for various dimensionless voltages across the system. Both for a reservoir concentration of 0.05 particles / nm^3 , length of $L = 333.0\text{nm}$ and relative membrane charge density of -5 . Near the membrane interface electro-neutrality breaks down.

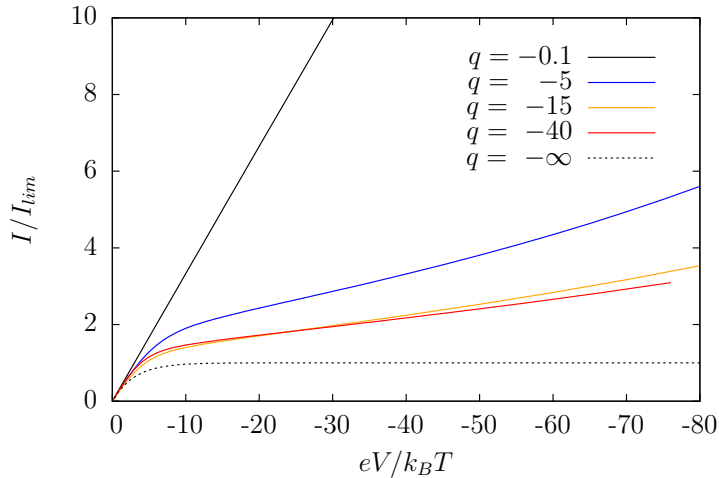


Figure 9: The I-V diagram for different values of q . Values were obtained at a reservoir concentration of $C_{res} = 0.05$ particles / nm^3 , a membrane width of $L = 333.0\text{nm}$. The value for $q = -\infty$ is the approximation from equation (8) with $V/3$, because we do not have a single wall any more, but a system three times as long.

For very small negative q we observe that the I-V curve becomes linear and our system will behave as an ohmic resistor with $V \sim R$. This is to be expected as we are then simply sending a current through a solution of positively and negatively charged particles.

As we go to higher voltages and exceed the limiting current we find that electro neutrality away from the bulk and the linearity of the potential breaks down. In Figure 11 we have plotted the potential for larger currents. This is in qualitative agreement with Figure 4. The potential is steepest and non-linear in the left diffusive layer. This must be counteracted by a net charge density because the current is constant across the system. We will examine this behaviour in the next section.

4.2.1 Extended space charge

For currents much higher than the limiting current, a peak in charge density will form away from the double layer in the left diffusive layer. This so called extended space charge (ESC) has been much investigated [11, 14]. In Figure 12 we have plotted this extended space charge density for varying values of V and q respectively. We see that the position of the peak is mostly determined by the voltage applied, while the intensity of the peak is mostly determined by q .

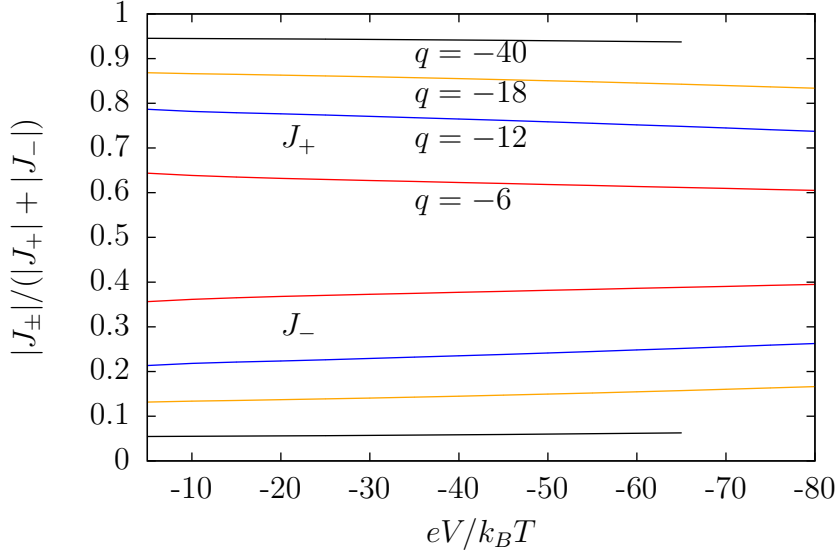


Figure 10: The relative contribution to the current of J_+ and J_- . Values were obtained at a reservoir concentration of $C_{res} = 0.05$ particles / nm^3 , a membrane width of $L = 333.0\text{nm}$ and a membrane charge density of $q = -5$.

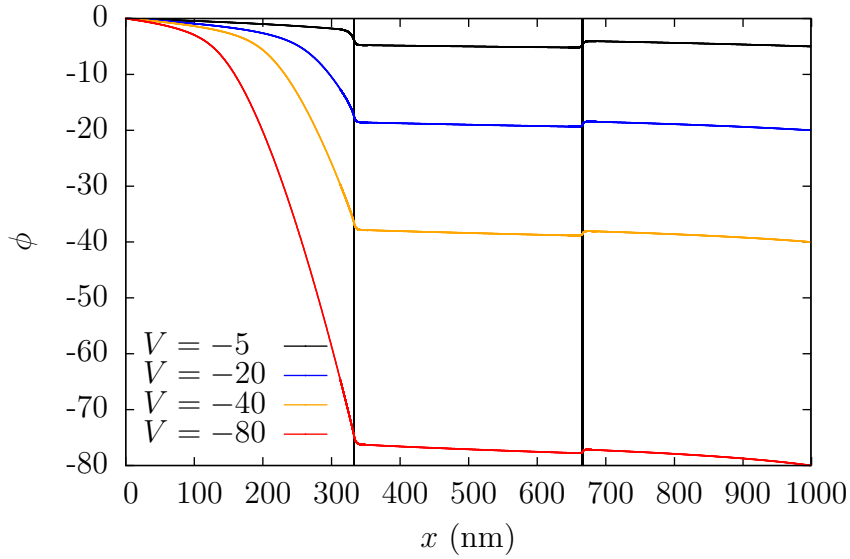


Figure 11: The dimensionless potential ϕ plotted for various higher voltages across the system. Values were obtained at a reservoir concentration of $C_{res} = 0.05$ particles / nm^3 , a membrane width of $L = 333.0\text{nm}$ and a membrane charge density of $q = -5$.

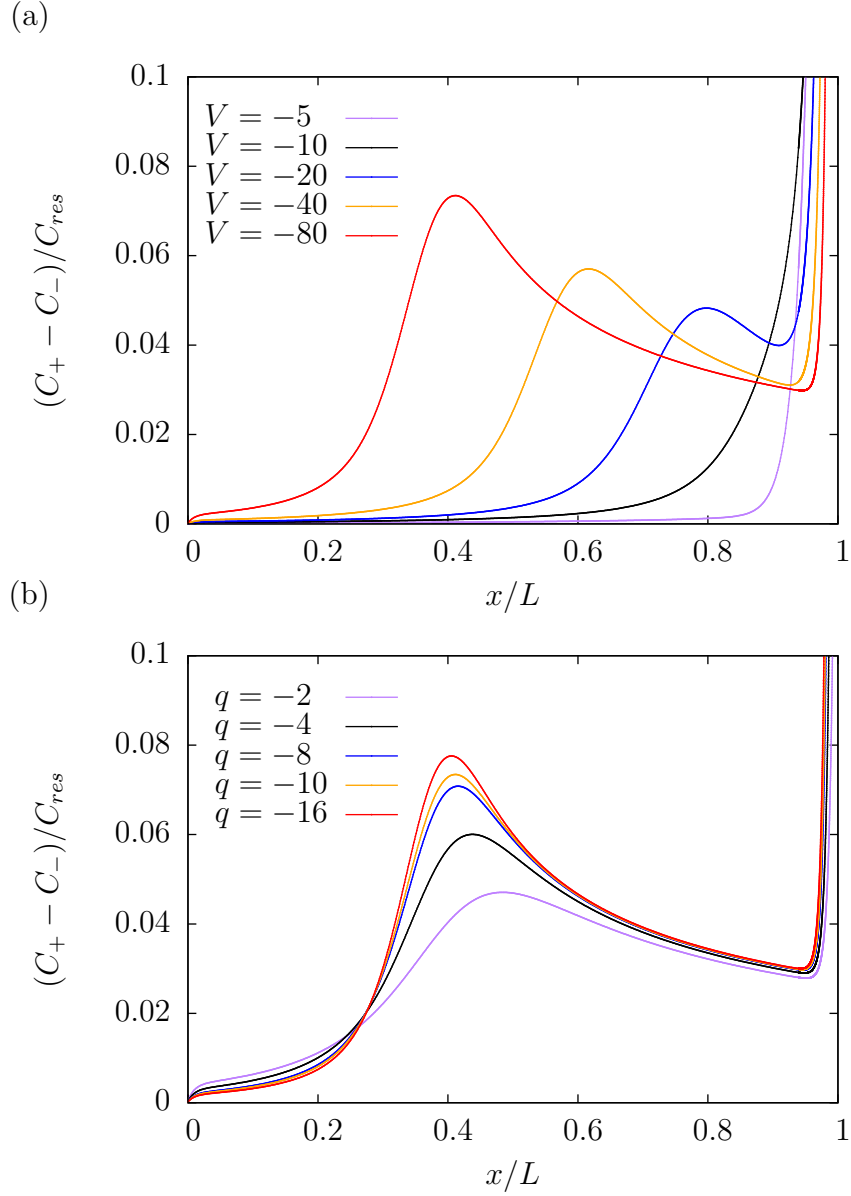


Figure 12: Relative charge density in the left diffusive layer for different values of (a) the applied dimensionless voltage V at membrane charge density of $q = -10$ and (b) for different values of the relative membrane charge density q obtained at a dimensionless voltage of $V = -80$. Both obtained at a membrane width of $L = 333\text{nm}$ and a reservoir concentration of $C_{res} = 0.005 / \text{nm}^3$.

5 Conclusion and discussion

Our results are in good agreement with reference [11] and qualitatively with reference [15]. The main feature of our model is the emergence of an extended space charge. Experimentally, a current much higher than the limiting current has been observed, and it is a long-standing question to explain this [15]. Several mechanisms have been proposed. One such mechanism is electro-osmotic instability (EOI) [16, 14]. Rubinstein and Zaltzmann found the extended space charge to be hydrodynamically unstable [17, 18]. Vortices of flow as a result of this instability have been predicted, and observed experimentally [19], although the theory remains to be tested quantitatively. While the extended space charge does form in our model, we do not take into account fluid flow and so we do not see these vortices. Chemical reactions in the electrolyte solution can also contribute to an increased current. At the membrane interfaces water splitting occurs, which leads to additional ions and thus conductivity [20, 21]. Another recently proposed mechanism is current induced membrane discharge (CIMD) [22]. Salt depletion in the membrane can lead to a pH shift, which in turns causes the membrane to discharge and lose selectivity. When we consider membranes as micro-channels such as in section 1 there are two additional mechanisms, namely surface conduction and electro-osmotic flow. For a comprehensive treatment of a micro-channel incorporating these mechanisms see reference [15].

The Poisson Nernst-Planck system for which numerical results were obtained in this thesis is thus just a starting point in describing the flow through an ion-selective membrane. Many mechanisms have been found to contribute to the current, and a quantitative correct theory in all regimes has not yet been found. To apply this knowledge on membranes to concentration-gradient engines and more specifically RED stacks, models consisting of micro-channels as the membrane and micro-pores as the capacitive porous electrode could be investigated.

References

- [1] R. S. Norman, “Water salination: A source of energy,” *Science*, vol. 186, no. 4161, p. 350, 1974.
- [2] B. E. Logan and M. Elimelech, “Membrane-based processes for sustainable power generation using water,” *Nature*, vol. 488, no. 7411, p. 313, 2012.
- [3] N. Boon and R. van Roij, “‘blue energy’ from ion adsorption and electrode charging in sea and river water,” *Molecular Physics*, vol. 109, no. 7, p. 1229, 2011.
- [4] H. V. M. Hamelers, O. Schaetzle, J. M. Paz-García, P. M. Biesheuvel, and C. J. N. Buisman, “Harvesting energy from co2 emissions,” *Environmental Science & Technology Letters*, vol. 1, no. 1, p. 31, 2014.
- [5] J. Paz-Garcia, O. Schaetzle, P. Biesheuvel, and H. Hamelers, “Energy from co2 using capacitive electrodes – theoretical outline and calculation of open circuit voltage,” *Journal of Colloid and Interface Science*, vol. 418, no. 0, p. 200, 2014.
- [6] T. Y. Cath, A. E. Childress, and M. Elimelech, “Forward osmosis: Principles, applications, and recent developments,” *Journal of Membrane Science*, vol. 281, no. 1–2, p. 70, 2006.
- [7] D. Brogioli, “Extracting renewable energy from a salinity difference using a capacitor,” *Phys. Rev. Lett.*, vol. 103, p. 058501, 2009.
- [8] J. Veerman, M. Saakes, S. Metz, and G. Harmsen, “Reverse electrodialysis: Performance of a stack with 50 cells on the mixing of sea and river water,” *Journal of Membrane Science*, vol. 327, no. 1–2, p. 136, 2009.
- [9] N. Y. Yip, D. A. Vermaas, K. Nijmeijer, and M. Elimelech, “Thermodynamic, energy efficiency, and power density analysis of reverse electrodialysis power generation with natural salinity gradients,” *Environmental Science & Technology*, vol. 48, no. 9, p. 4925, 2014.
- [10] M. students and M. Bazant, “Lecture 23: Ion concentration polarization.” MIT opencourseware (http://ocw.mit.edu/courses/chemical-engineering/10-626-electrochemical-energy-systems-spring-2011/lecture-notes/MIT10_626S11_lec23.pdf), 2011.

- [11] J. Manzanares, W. Murphy, S. Mafe, and H. Reiss, “Numerical simulation of the nonequilibrium diffuse double layer in ion-exchange membranes,” *The Journal of Physical Chemistry*, vol. 97, no. 32, p. 8524, 1993.
- [12] L. Thomas, “Elliptic problems in linear differential equations over a network: Watson scientific computing laboratory,” *Columbia Univ., NY*, 1949.
- [13] J. Anderson, *Computational Fluid Dynamics*. Computational Fluid Dynamics: The Basics with Applications, McGraw-Hill Education, 1995.
- [14] I. Rubinstein and B. Zaltzman, “Dynamics of extended space charge in concentration polarization,” *Phys. Rev. E*, vol. 81, p. 061502, 2010.
- [15] E. V. Dydek, B. Zaltzman, I. Rubinstein, D. S. Deng, A. Mani, and M. Z. Bazant, “Overlimiting current in a microchannel,” *Phys. Rev. Lett.*, vol. 107, p. 118301, 2011.
- [16] I. Rubinstein and B. Zaltzman, “Electro-osmotically induced convection at a permselective membrane,” *Phys. Rev. E*, vol. 62, p. 2238, 2000.
- [17] I. Rubinstein and B. Zaltzman, “Electro-osmotically induced convection at a permselective membrane,” *Phys. Rev. E*, vol. 62, p. 2238, 2000.
- [18] B. Zaltzman and I. Rubinstein, “Electro-osmotic slip and electroconvective instability,” *Journal of Fluid Mechanics*, vol. 579, p. 173, 2007.
- [19] S. M. Rubinstein, G. Manukyan, A. Staicu, I. Rubinstein, B. Zaltzman, R. G. H. Lammertink, F. Mugele, and M. Wessling, “Direct observation of a nonequilibrium electro-osmotic instability,” *Phys. Rev. Lett.*, vol. 101, p. 236101, 2008.
- [20] R. Simons, “Electric field effects on proton transfer between ionizable groups and water in ion exchange membranes,” *Electrochimica Acta*, vol. 29, no. 2, p. 151, 1984.
- [21] V. V. Nikonenko, N. D. Pismenskaya, E. I. Belova, P. Sistat, P. Huguet, G. Pourcelly, and C. Larchet, “Intensive current transfer in membrane systems: Modelling, mechanisms and application in electrodialysis,” *Advances in Colloid and Interface Science*, vol. 160, no. 1–2, p. 101, 2010.
- [22] M. B. Andersen, M. van Soestbergen, A. Mani, H. Bruus, P. M. Biesheuvel, and M. Z. Bazant, “Current-induced membrane discharge,” *Phys. Rev. Lett.*, vol. 109, p. 108301, 2012.